Biophysical Journal
Article

Biophysical Society

A Flux Balance of Glucose Metabolism Clarifies the Requirements of the Warburg Effect

Ziwei Dai,[1,2] Alexander A. Shestov,[3] Luhua Lai,[2] and Jason W. Locasale[1,*]
[1]Department of Pharmacology and Cancer Biology, Duke University School of Medicine, Duke Molecular Physiology Institute, Duke Cancer Institute, Durham, North Carolina; [2]Center for Quantitative Biology, Academy for Advanced Interdisciplinary Studies, Peking University, Beijing, China; and [3]Department of Radiology, Perelman School of Medicine, University of Pennsylvania, Philadelphia, Pennsylvania

ABSTRACT The Warburg effect, or aerobic glycolysis, is marked by the increased metabolism of glucose to lactate in the presence of oxygen. Despite its widespread prevalence in physiology and cancer biology, the causes and consequences remain incompletely understood. Here, we show that a simple balance of interacting fluxes in glycolysis creates constraints that impose the necessary conditions for glycolytic flux to generate lactate as opposed to entering into the mitochondria. These conditions are determined by cellular redox and energy demands. By analyzing the constraints and sampling the feasible region of the model, we further study how cell proliferation rate and mitochondria-associated NADH oxidizing and ATP producing fluxes are interlinked. Together this analysis illustrates the simplicity of the origins of the Warburg effect by identifying the flux distributions that are necessary for its instantiation.

INTRODUCTION

Aerobic glycolysis, or the Warburg effect, is defined as the production of lactate from glucose that occurs even in the presence of oxygen (1). It is a common feature of tumor and developing cells, and the measurement of glucose uptake through imaging using positron emission tomography with fluorodeoxy glucose (FDG-PET) is a common cancer diagnostic (2). The phenomenon is conserved across metazoans, and even Baker's yeast carries out fermentation in the presence of oxygen in specified conditions (3). The Warburg effect is positively regulated by oncogenes (e.g., *Myc*, *Kras*) and negatively regulated by tumor suppressor genes, such as *TP53* and *PTEN* (4).

It is generally considered a counterintuitive phenomenon. It is a less efficient mechanism of energy metabolism, since only two molecules of ATP are produced from one molecule of glucose. It also precludes the utilization of carbon for biomass since, by its definition, the secreted lactate is an end-product and cannot participate in biomass synthesis. Hypotheses on the function of the Warburg effect (5) include, but are not limited to, limitation of the total number of enzymes by molecular crowding (6–8); creation of an imbalance between NADPH and ATP production and consumption in biomass synthesis (2); requirement of rapid ATP generation for the transient energy demand of membrane transporters (9); or a consequence of competition with other cells in a population (10). Stoichiometric models of cellular metabolism are widely used in elucidating these hypotheses (11,12). However, these models tend to involve thousands of coupled algebraic equations and even more flux variables that often lead to difficulty in both reducing the dimensionality of feasible regions of the model and interpreting the resulting solutions. Also, mass-action-based kinetic models of glycolysis have lent insights into glucose metabolism, but these models contain large numbers of parameters, which can also limit their interpretation (13).

In this study, we consider a simple flux balance of glycolysis and identify the flux distributions that are necessary for the Warburg effect. We then integrate experimentally measured flux data into the analysis to illustrate the conditions that result in the Warburg effect and show the possible transitions that can occur from normal tissue physiology to that of aerobic glycolysis. This analysis provides a set of quantitative relationships for flux configurations necessary for aerobic glycolysis or oxidative metabolism in the mitochondria, and demonstrates a "redox-limited" mechanism of the Warburg effect. Our analysis reveals the central role of redox balancing in leading to the Warburg effect and its correlation to proliferation rate. We also construct the landscape of balanced fluxes in glucose metabolism to enable a global overview of quantitative relationships among the interacting fluxes. Despite its extreme simplicity, the model

Submitted April 21, 2016, and accepted for publication July 22, 2016.
*Correspondence: jason.locasale@duke.edu
Editor: Stanislav Shvartsman.
http://dx.doi.org/10.1016/j.bpj.2016.07.028

provides insights into the origin of the Warburg effect and is supported by multiple experimental studies.

MATERIALS AND METHODS

Evaluation of *k*

According to the molecular composition of cellular dry weight (DW) and number of serines, glycines, and one-carbon units needed to synthesize the precursors shown in Table S1 in the Supporting Material, 0.1675 mmol serine molecules, 0.7109 mmol glycine molecules, and 0.1750 mmol one-carbon units are needed to produce 1 gDW of cellular material. Since serine produced by J_{out} can be either directly used in synthesizing proteins or form glycine and one-carbon units, the total amount of serine needed can be calculated by

$$\begin{aligned} C_{\mathrm{Ser}}^{\mathrm{total}} &= C_{\mathrm{Ser}} + \max\left(C_{\mathrm{Gly}}, C_{\mathrm{C1}}\right) = 0.1675 + 0.7109 \\ &= 0.8784(\mathrm{mmol/gDW}). \end{aligned} \tag{1}$$

Let $m(t)$ be the total DW of cells at time t and $S(t)$ be the total amount of serine consumed in the synthesis of $m(t)$, and we have

$$\frac{dS(t)}{dt} = J_{\mathrm{out}} m(t) = k\mu \mathrm{m}(t), \tag{2}$$

$$\frac{dm(t)}{dt} = \mu \mathrm{m}(t). \tag{3}$$

Dividing Eq. 2 by Eq. 3, we have

$$k = \frac{dS(t)}{dm(t)} = C_{\mathrm{Ser}}^{\mathrm{total}} = 0.8784\ \mathrm{mmol/gDW}. \tag{4}$$

Under the assumption that 1 gDW = 4 gWW, $k \approx 219.6\ \mu$mol/gWW.

Sampling feasible flux configurations

Rewriting the flux-balance model as matrix equations,

$$\begin{bmatrix} 1 & -(k+A) & \alpha & 0 & 0 \\ 1 & k & 0 & -1 & -1 \\ 1 & -k & -1 & 0 & -1 \end{bmatrix} \begin{bmatrix} J_{\mathrm{in}} \\ \mu \\ J_{\mathrm{Ox}} \\ J_{\mathrm{N}} \\ J_{\mathrm{Lac}} \end{bmatrix} = \begin{bmatrix} m \\ 0 \\ 0 \end{bmatrix}. \tag{5}$$

Rearranging the fluxes, we have

$$\begin{bmatrix} -(k+A) & \alpha & 0 \\ k & 0 & -1 \\ -k & -1 & -1 \end{bmatrix} \begin{bmatrix} \mu \\ J_{\mathrm{Ox}} \\ J_{\mathrm{Lac}} \end{bmatrix} = \begin{bmatrix} m \\ 0 \\ 0 \end{bmatrix} - \begin{bmatrix} 1 & 0 \\ 1 & -1 \\ 1 & -1 \end{bmatrix} \begin{bmatrix} J_{\mathrm{in}} \\ J_{\mathrm{N}} \end{bmatrix}. \tag{6}$$

According to Eq. 6, we can directly solve the linear equations to calculate μ, J_{Ox},and J_{Lac} from J_{in} and J_{N}. We sampled 50,000 combinations of J_{in} and J_{N} in the range $J_{\mathrm{in}} \in [0\ \mu\mathrm{mol/gWW/min}, 4\ \mu\mathrm{mol/gWW/min}], J_{\mathrm{N}} \in [0\ \mu\mathrm{mol/gWW/min},\ 2.6\ \mu\mathrm{mol/gWW/min}]$ by Latin hypercube sampling and calculated the remaining fluxes by solving Eq. 6. Only the flux configurations with all fluxes nonnegative were kept. The ranges of J_{in} and J_{N} sampled were set according to upper limits of these fluxes reported in the literature (Table S2).

Accessing The Cancer Genome Atlas breast tumor data set

Pancan-normalized RNaseq data of breast invasive carcinoma in The Cancer Genome Atlas were downloaded using the cancer genome browser (https://genome-cancer.ucsc.edu) (14,15). The data set includes gene expression profiles measured by RNA-sequencing for 1095 breast tumors and 113 adjacent normal samples. The list of genes involved in the Kyoto Encyclopedia of Genes and Genomes (KEGG) pathways "Metabolic pathways," "Glycolysis/gluconeogenesis," "TCA cycle," and "Oxidative phosphorylation" were extracted from the KEGG database (16) using the KEGG application programming interface (API).

Constructing and solving the growth-rate-maximization models

Under the assumption that the cell determines the flux configuration by maximizing the growth rate, μ, we can write the flux-balance model into a linear programming problem:

$$\max \mu, s.t. \quad \begin{bmatrix} 1 & 1 & -1 & -1 & 0 & 0 & 0 \\ 1 & -1 & -1 & 0 & -1 & 0 & 0 \\ -1 & 1 & 0 & 0 & -\alpha & 1 & 0 \\ 0 & 1 & 0 & 0 & 0 & 0 & -k \\ 0 & 0 & 0 & 0 & 0 & 1 & -A \end{bmatrix} \begin{bmatrix} J_{\mathrm{in}} \\ J_{\mathrm{out}} \\ J_{\mathrm{Lac}} \\ J_{\mathrm{N}} \\ J_{\mathrm{Ox}} \\ J_{\mathrm{A}} \\ \mu \end{bmatrix} = \begin{bmatrix} 0 \\ 0 \\ 0 \\ 0 \\ m \end{bmatrix}.$$

$$\begin{cases} 0 \le J_{\mathrm{in}} \le J_{\mathrm{in}}^{\mathrm{ub}} \\ 0 \le J_{\mathrm{out}} \le J_{\mathrm{out}}^{\mathrm{ub}} \\ 0 \le J_{\mathrm{Lac}} \le J_{\mathrm{Lac}}^{\mathrm{ub}} \\ 0 \le J_{\mathrm{N}} \le J_{\mathrm{N}}^{\mathrm{ub}} \\ 0 \le J_{\mathrm{Ox}} \le J_{\mathrm{Ox}}^{\mathrm{ub}} \\ 0 \le J_{\mathrm{A}} \le J_{\mathrm{A}}^{\mathrm{ub}} \\ \mu \ge 0 \end{cases} \tag{7}$$

The upper limits on the fluxes were generated by enumerating a combination of 50 different values of $J_{\mathrm{in}}^{\mathrm{ub}}$ ranging from 0.2 μmol/gWW/min to 10 μmol/gWW/min and 50 different values of $J_{\mathrm{N}}^{\mathrm{ub}}$ ranging from 0.1 μmol/gWW/min to 5 μmol/gWW/min (see Fig. 4, *A* and *B*) or randomly generating 10,000 combinations of $(J_{\mathrm{in}}^{\mathrm{ub}}, J_{\mathrm{out}}^{\mathrm{ub}}, J_{\mathrm{Lac}}^{\mathrm{ub}}, J_{\mathrm{N}}^{\mathrm{ub}}, J_{\mathrm{Ox}}^{\mathrm{ub}}, J_{\mathrm{A}}^{\mathrm{ub}})$ by Latin hypercube sampling in which all upper limits range from 0 μmol/gWW/min to 10 μmol/gWW/min (see Fig. 4 *C*). We also added random solvent capacity constraints to the randomly generated 10,000 models:

$$w_1 J_{\mathrm{in}} + w_2 J_{\mathrm{out}} + w_3 J_{\mathrm{Lac}} + w_4 J_{\mathrm{N}} + w_5 J_{\mathrm{Ox}} + w_6 J_{\mathrm{A}} \le 50. \tag{8}$$

All weight coefficients were sampled from a log-normal distribution: $\log_{10} w_i \sim N(0,1)$. Linear programming problems were solved by the MOSEK optimization toolbox for MATLAB (17).

RESULTS

Flux analysis of glycolysis

We first considered a balance of the fluxes in glycolysis (Fig. 1 *A*). The three fluxes involved in glucose metabolism (carbon flow, energy flow, and redox status involving NAD^+/NADH) are constrained to mass conservation relationships: i.e., at steady state, the rate of glucose entering glycolysis equals the total rate of glucose leaving glycolysis, the rate of oxidation of NADH equals the rate of NAD^+ reduction, and the rate of ATP synthesis equals the rate of ATP consumption. These fluxes interact during glycolysis when the carbon backbone derived from glucose is coupled to either a redox reaction (i.e., catalyzed by glyceraldehyde phosphate dehydrogenase (GAPDH) or lactate dehydrogenase (LDH)) or an ATP-coupled process such as oxidative phosphorylation or phosphorylation of ADP by pyruvate kinase. This flux balance results in three equations (Fig. 1 *B*). A variable can be defined that quantifies the extent of the Warburg effect through the ratio of flux to lactate (J_{Lac}) to flux of pyruvate into the mitochondria (J_{ox}). We should note that other fluxes such as pyruvate carboxylase or incomplete oxidation of glucose in the mitochondria arising from, for example, biosynthesis, would alter terms in these equations, but the overall balance would remain the same. These processes, although often essential for cell viability, are typically small compared to the other fluxes considered.

For the balance of glucose, the equation is

$$\frac{d[\mathrm{Carbon}]}{dt} = J_{\mathrm{in}} - J_{\mathrm{out}} - J_{\mathrm{Lac}} - J_{\mathrm{Ox}} = 0, \qquad (9)$$

where [Carbon] is the concentration of carbon that enters lower glycolysis, J_{in} is the flux of glucose that has entered lower glycolysis, defined as having undergone oxidative phosphorylation by GAPDH, J_{out} is the flux of glucose-derived carbon atoms leaving glycolysis through phosphoglycerate dehydrogenase (PHGDH), J_{Lac} is the flux of glucose leaving as lactate, J_{Ox} is the flux of glucose entering the mitochondria. Note that the convention of glucose uptake in this scenario is such that ATP generation through glycolysis is net zero at this point, immediately before the GAPDH step, since the flux through pyruvate kinases that generates a net production of ATP has not yet occurred.

For ATP metabolism and energy balance, the equation is

$$\frac{d[\mathrm{ATP}]}{dt} = J_{\mathrm{PK}} + \alpha J_{\mathrm{Ox}} - J_{\mathrm{A}} = 0, \qquad (10)$$

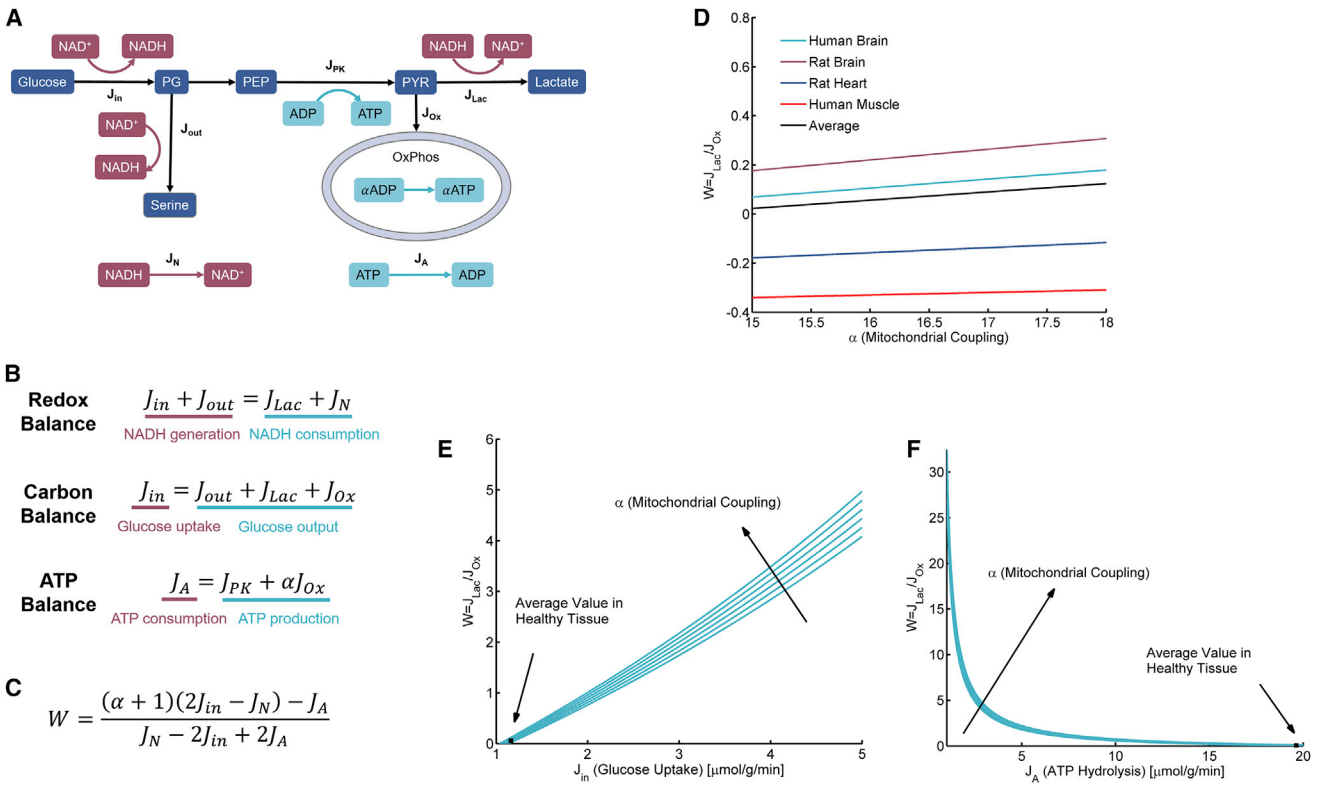

FIGURE 1 The flux-balance model of glycolysis demonstrates how the Warburg effect is affected by fluxes in glucose metabolism. (*A*) Flux-balance model of glycolysis. (*B*) Equality constraints for balance of NADH, carbon, and ATP. (*C*) Expression of the extent of the Warburg effect by fluxes J_{in}, J_{N}, and J_{A}. (*D*) Analysis of the Warburg effect in healthy tissues. Negative values of W imply that carbon sources other than glucose are required to match cellular ATP demand. (*E* and *F*) Effects of increasing glucose uptake, increasing mitochondrial coupling or decreasing ATP turnover on the shift from oxidative phosphorylation to aerobic glycolysis. To see this figure in color, go online.

where [ATP] is the concentration of intracellular ATP, α is the extent of mitochondrial coupling of the citric (tricarboxylic) acid (TCA) cycle to oxidative phosphorylation per unit of carbon entering the TCA cycle (α is thought to be between 15 and 18 for a completely coupled mitochondrion), J_{PK} is the flux through pyruvate kinase that generates a unit of ATP, and J_A is the combined rate of ATP hydrolysis that arises from the sum total of ATP-consuming processes in cells. Furthermore, J_{PK} can be estimated from J_{in} and J_{out} considering the balance of fluxes passing phosphoenolpyruvic acid (PEP):

$$\frac{d[\mathrm{PEP}]}{dt} = J_{in} - J_{out} - J_{PK} = 0. \tag{11}$$

Incorporating Eq. 11 into Eq. 10, then, the equation for [ATP] is

$$\frac{d[\mathrm{ATP}]}{dt} = J_{in} - J_{out} + \alpha J_{Ox} - J_A = 0. \tag{12}$$

For the NAD^+ metabolism and redox balance in the cytosol, the equation is

$$\frac{d[\mathrm{NADH}]}{dt} = J_{in} + J_{out} - J_{Lac} - J_N = 0, \tag{13}$$

where [NADH] is the concentration of cytosolic intracellular NADH and J_N is the rate of NADH turnover due to the sum total of NADH-oxidizing reactions that occur in the cytosol. Note that the mitochondrial NADH shuttles can transport NADH between the mitochondria and cytosol, thus affecting the redox balance in the cytosol. The majority of J_N is carried by the malate-aspartate shuttle (MAS), which is able to translocate electrons produced in glycolysis to mitochondria by oxidizing NADH in the cytosol and reducing NAD^+ in mitochondria. Although the MAS is coupled to the mitochondria, these equations account only for the mass balance in the cytosol. Thus, the mitochondria are implicitly involved in this model by defining J_N and J_{Ox}. Since evidence from proteomics data suggests that the abundance of glycolytic enzymes exceeds that of enzymes associated with any other metabolic pathways, and GAPDH and LDH comprise most of the total concentration of enzymes catalyzing NADH-mediated reactions (18), other reactions in the cytosol that produce NADH were ignored for simplicity, but all other reactions consuming NADH in the cytosol were subsumed in the J_N term.

Note that there are three algebraic equalities that impose constraints and six fluxes. Thus, three of the fluxes can be considered as independent variables. By rearranging these equations, we can derive expressions for the extent of the Warburg effect, defined as the ratio of flux to lactate over the flux of pyruvate into the mitochondria ($W = (J_{Lac}/J_{Ox})$). Different choices of the independent variables can yield different interpretations of aerobic glycolysis, which will be discussed in depth in the next sections.

Relationship to fluxes in healthy tissue

After choosing a representation using J_A, J_{in} and J_N, fluxes with abundant experimental values in literature, we first considered them as independent variables to obtain a view of the extent of the Warburg effect in different tissues:

$$W = \frac{(\alpha+1)(2J_{in} - J_N) - J_A}{J_N - 2J_{in} + 2J_A}. \tag{14}$$

When measured fluxes are used in Eq. 14, one can estimate the extent of the Warburg effect in different tissues. We note that these fluxes in practice are not necessarily independent; however, the measurements from literature are independent, allowing for analysis of these terms as independent variables. We surveyed a large set of literature measurements of fluxes in human and animal tissues on the rate of ATP turnover (J_A), the rate of the TCA cycle (approximation of J_N) and the absolute glucose uptake rate (approximation of $0.5J_{in}$). Fluxes were converted to standardized units (μmol/gWW/min). A different conversion factor relating DW to wet weight (WW) was considered depending on the tissue (liver, 4 gWW = 1 gDW; muscle, 4.2 gWW = 1 gDW; heart, 5.5 gWW = 1 gDW). For the case of brain tissue, the value is always given in gWW (19–21). Note that the conversion factor may vary slightly due to experimental procedures in measuring the fluxes and variation in tissue water content among different studies, but the variation is small compared to its absolute value, since the water content is very similar in these tissues, and thus is unlikely to affect the extent of the Warburg effect estimated from the fluxes (22,23). The fluxes and corresponding references are shown in Table S2.

Incorporating these values into the equations revealed that under conditions of healthy tissue physiology, typical values of the Warburg effect (W) are <0.10, meaning that $<10\%$ of the glucose is converted to lactate. Averaging the flux rates for different tissue types resulted in a value of $W < 0.3$ in each type of tissue with experimental values available for all independent variables J_{in}, J_A, and J_N (Fig. 1 *C*), which is in line with findings that healthy tissues mainly rely on mitochondrial oxidative phosphorylation for energy demands. Since flux values estimated from the literature have multiple sources of noise due to factors including variation in the conversion from WW to DW and inconsistency between the measured and accurate flux values, we conducted a perturbation analysis to assess the robustness of the conclusion to variation of the fluxes, in which the flux values estimated from the literature were randomly perturbed near their original values to generate new flux configurations for estimation of the Warburg effect extent. The fluxes were perturbed by either increasing or decreasing

their values to up to fivefold. Most randomly perturbed flux configurations still exhibit $W < 0.1$ in all types of tissue (Fig. S1 in the Supporting Material), thus supporting the robustness of the conclusion to flux variations in large variations in literature values of metabolic fluxes.

Next we identified variation in fluxes yielding the Warburg effect by analyzing the trends of W changing with the fluxes. The effect of increasing glucose uptake is plotted in Fig. 1 *E*, and it is observed that flux configurations with 10- to 100-fold increases in glucose consumption (while other fluxes remain unchanged) are sufficient to exhibit the Warburg effect. The effect of decreasing ATP turnover is plotted (Fig. 1 *F*), and it is observed that an ~10-fold decrease in ATP turnover is associated with the Warburg effect. Together, these calculations define in both quantitative and qualitative terms the necessary and sufficient flux distributions that are required to yield the Warburg effect.

It is worth noting that these fluxes may not be independent; for instance, increasing the proliferation rate can result in an increase in both J_A and J_{in}, which means that varying one flux while keeping other fluxes fixed is unlikely to take place in reality. In the next sections, we introduce proliferation rate to further reduce dimensionality of the model's feasible region. We also focus on constraints introduced by flux balancing to derive more rigorous relationships, which is robust to dependence of the fluxes not involved in the model.

Role of redox balance in the Warburg effect and cell growth

Now, if we let J_{in}, J_{out}, and J_N be the independent variables, the extent of the Warburg effect, W, can be written as

$$W = \frac{J_{in} + J_{out} - J_N}{J_N - 2J_{out}}. \quad (15)$$

Note that in this expression, $J_{in} + J_{out}$ is the total NADH production in glycolysis and serine synthesis, whereas J_N is the total NADH-consuming flux, separate from that of lactate production from pyruvate. As the equation shows, the Warburg effect ($W > 0$) will be necessary when the rate of NADH generated in glycolysis and serine synthesis is not balanced entirely by J_N. Since J_N mainly consists of the flux of the MAS, it is limited by the metabolic activity of the mitochondria.

Note that J_{out} is the rate of serine synthesis that is involved in multiple biosynthetic pathways (24). For a further illustration, if we assume that growth is limited by the generation of biomass precursors from glucose such as the purines and pyrimidines obtained from serine synthesis, then the growth rate, μ, is proportional to J_{out}:

$$J_{out} = k\mu. \quad (16)$$

Such a consideration may hold in certain cases when glucose is the predominant nutrient being utilized for the generation of biomass, as has been hypothesized to occur in growing tumors (2). Although other precursors, such as amino acids other than serine and intermediates of the TCA cycle and pentose phosphate pathway, also contribute significantly to biomass production, it is still reasonable to expect that J_{out} and μ are related, since serine contributes to multiple cellular building blocks. The simplest way to model this relationship quantitatively is to assume that the growth rate is proportional to J_{out}. From this linear relationship and the fact that J_{Ox} cannot be negative, we have $\mu \leq (J_N/2k)$, which implies that cellular growth rate would be limited by the activity of NAD^+ regenerating enzymes. The finding that J_{out} is limited by J_N is consistent with the positive correlation of expression levels of genes malate dehydrogenase 1 (MDH1), the main enzyme that turns over NADH in the MAS, and PHGDH, the initating enzyme from glycolysis to de novo serine biosynthesis in human breast tumors (Spearman's rank correlation $\rho = 0.3825$, $p = 1.32 \times 10^{-43}$; Fig. 2 *A*). The positive correlation between the mean expression levels of genes involved in the MAS and the expression level of PHGDH is also significant (Spearman's rank correlation $\rho = 0.2447$, $p = 5.06 \times 10^{-18}$; Fig. 2 *B*). The Spearman's rank correlation coefficients between genes in de novo serine synthesis and genes associated with the MAS are higher compared to that between the expression level of PHGDH (Fig. 2 *C*), MDH1 (Fig. 2 *D*), or MAS-associated genes (Fig. 2 *E*) and most of the other metabolic genes involved in the KEGG pathway Metabolic pathways. The correlation is also significant in comparison to correlation with genes associated with glycolysis, the TCA cycle, and oxidative phosphorylation (Fig S2). Noisiness in the correlation results is likely from numerous factors, including but not limited to the difficulty in obtaining reliable measurements of mRNA transcripts in primary tumors, the heterogeneity of cell types in tumor data, and the discrepancy between levels of transcripts, protein levels, and metabolic fluxes that result from enzyme activity.

In summary, according to our flux-balance considerations, the demand of restoring oxidative power by regenerating NAD^+ from NADH produced in glycolysis and serine synthesis affects regulation of glycolysis and central carbon metabolism in multiple ways. It forces lactate production from glucose as compensation if the redox demand cannot be satisfied by the mitochondria-coupled MAS alone. It also limits the capacity of de novo serine synthesis, thus limiting cell proliferation due to net production of NADH in these processes.

Role of proliferation and redox balance in central carbon metabolism

The coefficient k in Eq. 16 can be evaluated from the biomass composition of human cells in literature and from

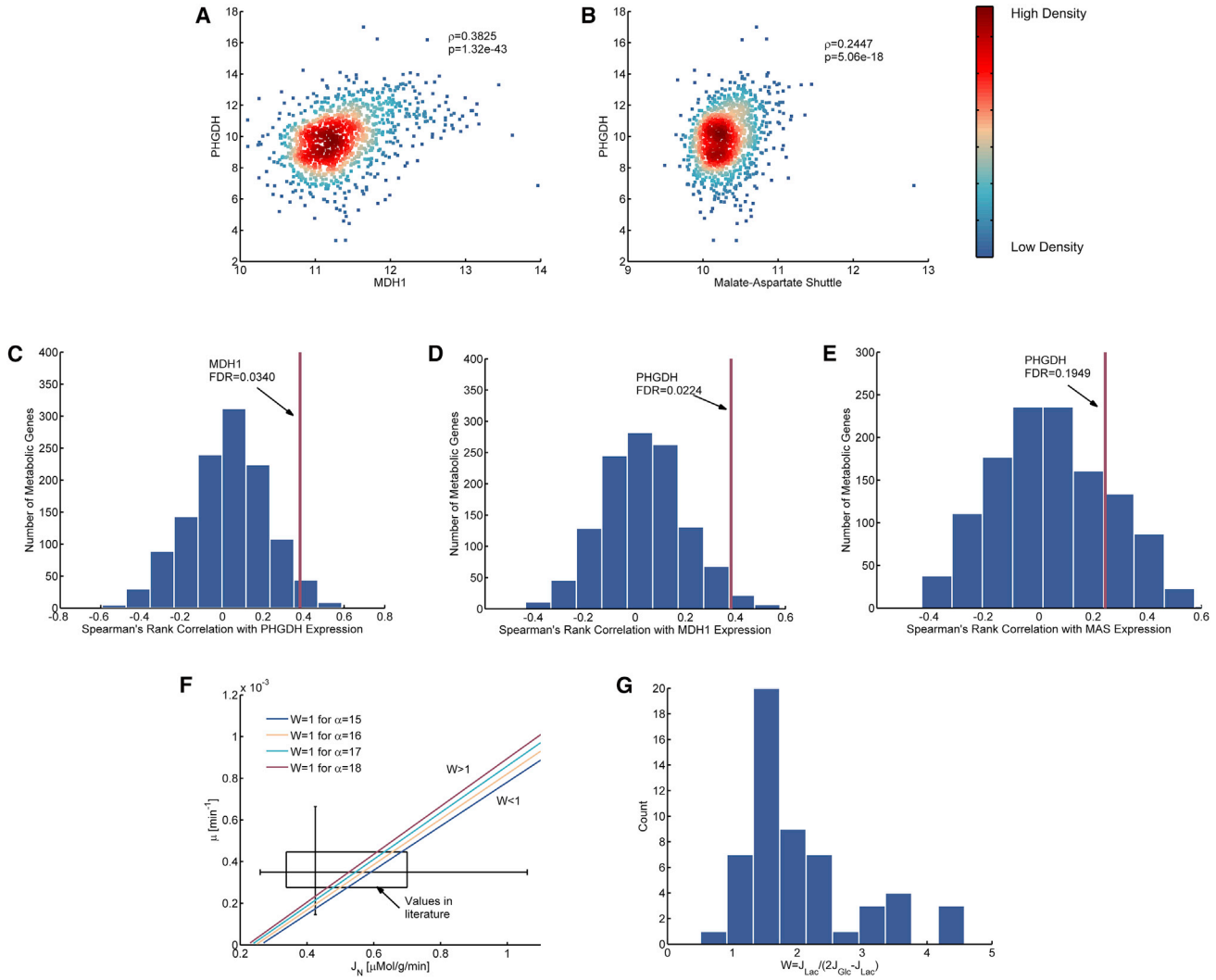

FIGURE 2 The interplay of redox balancing and proliferation in regulating aerobic glycolysis. (*A* and *B*) Correlation of PHGDH and malate-aspartate shuttle at single gene and pathway level among breast tumor samples in the Cancer Genome Atlas. Color in the scatter plot represents density of points. (*C–E*) Comparison of correlations shown in (*A*) and (*B*) between the expression of PHGDH, MDH1, and MAS and other metabolic genes involved in the KEGG pathway databased termed 'Metabolic Pathways'. The false discovery rate (FDR) values were defined as the fraction of 'background' correlations larger than that between PHGDH and MDH1 or between PHGDH and MAS. (*F*) Two-dimensional box plot shows the distribution of JN and μ estimated from data reported in literature. (*G*) Distribution of W evaluated for NCI-60 cell lines from exchange flux rates. The W=1 line connecting the NADH oxidizing flux JN and the growth rate μ. Different colors represent different values of α. To see this figure in color, go online.

the stoichiometry in the serine-glycine synthesis and one-carbon metabolism. For simplicity, we ignored the glycine cleavage system, whose contribution in replenishing the one-carbon pool is often much smaller than that of serine hydroxymethyltransferase (SHMT) (25,26), and uptake of serine and glycine, which will decouple J_{out} with the downstream fluxes. A particular value of k was observed to be 219.6 μmol/gWW and the parameters used in evaluating it are listed in Table S1.

The energy utilization rate, J_A, can be decomposed into two parts consisting of a term for the rate of energy consumed in growth-related processes and a term for the energy consumption rate for processes involved in cellular maintenance (27,28), such as the maintenance of ion gradients, intracellular trafficking, synthesis of housekeeping proteins, etc.:

$$J_A = m + A\mu, \tag{17}$$

where $A\mu$ is the energy rate used in biosynthesis, with A being the factor that couples energy rate with growth rate and m the maintenance energy rate. By considering two equality constraints connecting μ and two fluxes, we can further reduce the degrees of freedom to two. Let J_N and μ be the independent variables; then, W becomes

$$W = \frac{[2(\alpha+1)k + A]\mu + m - (\alpha+1)J_N}{J_N - 2k\mu}. \tag{18}$$

Thus, W is a monotonically increasing function of μ and a decreasing function of J_N. For $W = 1$, we have

$$\mu_{W=1} = \frac{(\alpha+2)J_N - m}{2(\alpha+2)k + A}. \quad (19)$$

We can also write J_N as a linear function of μ for $W = 1$:

$$J_{N,W=1} = \frac{[2(\alpha+2)k + A]\mu + m}{\alpha+2}. \quad (20)$$

Here, $W > 1$ means that the glucose flux diverted to lactate production exceeds the flux entering oxidative phosphorylation in the mitochondria, thus providing a quantitative definition of the Warburg effect. For simplicity, let μ_W denote $\mu_{W=1}$ and J_{NW} denote $J_{N,W=1}$. Since W increases with μ and decreases with J_N, it is apparent that for $\mu > \mu_W$ or $J_N < J_{NW}$, W will be >1 and the Warburg effect will be exhibited. It can be interpreted as a "proliferation-induced" (considering $\mu > \mu_W$) or redox-limited (considering $J_N < J_{NW}$) Warburg effect.

To connect these relationships with cellular physiology, we estimated the values for parameters k, A, and m in (19) and (20) from the literature. Values of A and m can be evaluated by measurements of ATP production under varying growth rates and have been found to be $A = 8625$ μmol/gWW and $m = 4.427$ μmol/gWW/min (27). With these parameters, the $W = 1$ line is determined (Fig. 2 *F*). This line separates the (J_N,μ) plane into two parts: in the upper left part, $W > 1$ holds, and in the lower right part, $W < 1$ holds.

We collected data for doubling time of the NCI-60 cell lines to evaluate distribution of growth rate μ in cancer cells, which usually show significant aerobic glycolysis. Since we don't have data for J_N in the NCI-60 cell lines, we evaluated the distribution of J_N from flux through the MAS in mammalian cells, reported in the literature(Table S2). The two-dimensional box plot in Fig. 2 *F* shows the distribution. Comparing the $W = 1$ line and the distribution of J_N and μ, we were able to conclude that the majority of the distribution lies on the $W > 1$ part. In other words, for the NCI-60 cell lines, if the NADH-oxidizing flux in the cytosol is comparable to the flux through the MAS, reported in the literature, the cell lines have a tendency to show the Warburg effect. We calculated W for the cell lines by $W = J_{Lac}/(2J_{Glc} - J_{Lac})$ according to exchange fluxes of glucose and lactate (Fig. 2 *G*) (29). Consistent with our results, all cell lines except one showed $W > 1$, which supports proliferation-induced, or redox-limited, aerobic glycolysis as a plausible mechanism of the Warburg effect.

A global map of flux balance in glycolysis

As mentioned, by introducing a growth rate, μ, and coupling it with J_{out} and J_A, two independent variables are sufficient to describe the distribution of feasible flux configurations. We constructed such a "landscape of flux configurations" by sampling the feasible region of the flux-balance model using Latin hypercube sampling and considering its projection on different binary combinations of μ, J_{in}, J_{Ox}, J_N, and J_{Lac} (Fig. 3 *A*). For the details of the sampling procedure, see Materials and Methods.

This global map affords a clear illustration of flux couplings by stoichiometry and their contribution to the Warburg effect. For example, it shows that increasing J_{in} under fixed J_{Ox}, J_N, or μ will lead to increasing aerobic glycolysis. The only exception about the effect of increasing J_{in} on W is that increasing J_{in} while keeping J_{Lac} unchanged will reduce the Warburg effect, since the increment of J_{in} will be diverted to J_{out} or J_{Ox}. However, in the projection onto J_{in} and J_{Lac}, the minimal W under fixed J_{in} increases with increasing J_{in}, which also demonstrates the important role of increasing glucose uptake in inducing the Warburg effect.

Another key aspect of this global-flux configuration map is the tight correlation among J_N, μ, and J_{Ox}. This relationship could be intuitively derived from the equality constraints. By subtracting Eq. 13 from Eq. 9 and replacing J_{out} with $k\mu$, we have

$$J_{Ox} = J_N - 2k\mu. \quad (21)$$

Thus, if two of the three variables J_{Ox}, J_N, and μ are linearly coupled, each will be linearly coupled. Due to the assumed linear coupling of J_A and μ, μ is approximately linear to J_{Ox} if the mitochondria-related term αJ_{Ox} comprises most of the total ATP production flux, J_A. We calculated the fraction of glucose-derived carbon atoms entering the mitochondria, $W/(W+1)$, and the fraction of ATP produced in mitochondrial oxidative phosphorylation, $\alpha J_{Ox}/J_A$, for 20,000 flux configurations uniformly sampled in the feasible region of the model. Despite the fact that a substantial fraction of the flux configurations exhibit significant Warburg effect (Fig. 3 *F*), in most flux configurations, the majority of the ATP is produced in mitochondria (Fig. 3 *G*). Since J_{Ox} is linear to the ATP yield in mitochondria, which is approximately the total energy requirement that is linear to the growth rate, J_{Ox} is also approximately linear to the growth rate, μ. To summarize, the coupling among growth rate and mitochondria-related fluxes J_N and J_{Ox} is a direct consequence of high energy demand associated with rapid proliferation.

To test the hypothesis that cell proliferation is in part determined by J_N, we compared expression levels of MAS-related genes in NCI-60 cell lines and growth rate measurements. As shown in Fig. 3 *B*, the average expression levels of genes associated with the MAS (MDH1, MDH2, GOT1, GOT2, SLC25A11, SLC25A12, and SLC25A13) positively correlated with growth rate in cancer cells. For J_{Ox}, we used the average expression level of

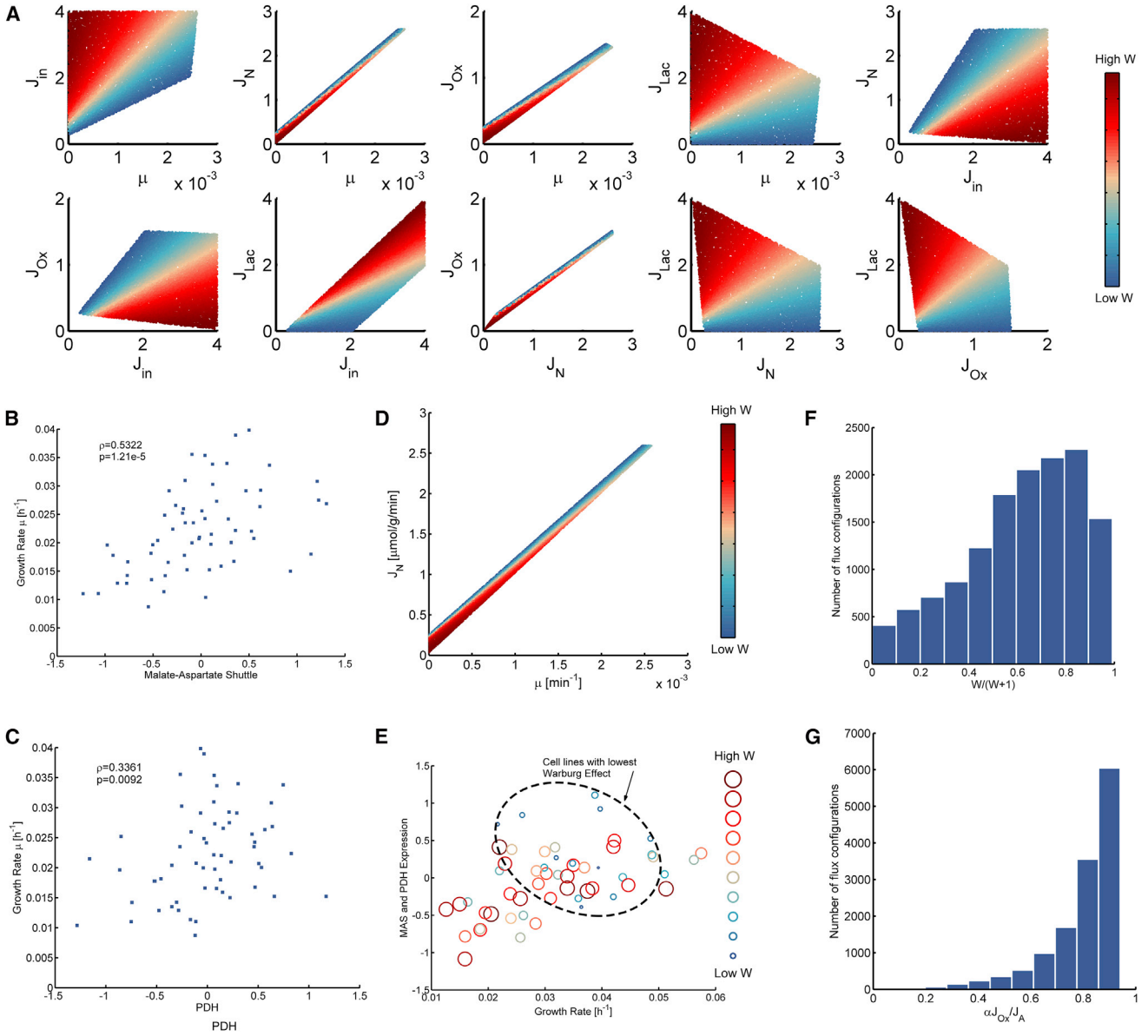

FIGURE 3 Landscape of balanced fluxes in central carbon metabolism. (*A*) Distribution of feasible flux configurations and their relative level of the Warburg effect defined as the rank of W among all sampled flux configurations. W increases as the color changes from blue to red. Mitochondrial coupling α=16 was used in the sampling. (*B*) Correlation of expression of malate-aspartate shuttle-associated genes and growth rate of NCI-60 cell lines. (*C*) Correlation of pyruvate dehydrogenase expression with growth rate in NCI-60 cell lines. (*D*) Interplay of proliferation and mitochondria-coupled NADH-oxidizing flux in determining the extent of aerobic glycolysis. (*E*) Relative strength of aerobic glycolysis of NCI-60 cell lines projected on growth rate and average expression level of MAS and PDH-related genes. (*F*) Distribution of $W/(W+1)$ among 20,000 randomly sampled flux configurations. (*G*) Distribution of $\alpha J_{Ox}/J_A$ among 20,000 randomly sampled flux configurations. To see this figure in color, go online.

pyruvate-dehydrogenase (PDH)-related genes to approximate it. Comparing the expression level of PDH and growth rate, we also observed a statistically significant positive correlation between them, which further supports this model. The correlations between growth rate and the MAS and PDH expression values are significant in comparison to correlations between growth rate and genes involved in the KEGG pathway Metabolic pathways, Glycolysis/gluconeogenesis, TCA cycle, and Oxidative phosphorylation (Fig S3). Variation of the parameters obtained from Latin hypercube Monte Carlo sampling changes the shape of the feasible region, but the correlation and how the extent of Warburg effect changes with the fluxes is not affected (Fig S4).

Interplay between proliferation and mitochondria activity in determining the Warburg effect

The global map of flux balance described in the section above can give a clear illustration of the relationship

between proliferation and NADH turnover, as well as the way they regulate aerobic glycolysis. As Fig. 3 *D* shows, although increasing proliferation rate μ under the same J_N leads to higher W, the current value of J_N will limit μ from further increasing. Further increasing μ requires a concomitant increase of J_N, which has the opposite effect on aerobic glycolysis. The interaction of these two effects in combination attenuates aerobic glycolysis, as shown in Fig. 3 *D*, where the flux configurations in the top right corner of the feasible region show less aerobic glycolysis compared to those in the bottom left part. The trend of the Warburg effect changing with μ and J_{Ox} is similar, since increasing μ also requires an increase of J_{Ox} due to the energy demand in proliferation (Fig. 3 *A*). For the NCI-60 cell lines (Fig. 3 *E*), we approximated the mitochondrial activity by the average expression level of MAS and PDH genes and showed how the extent of the Warburg effect varies with growth rate and mitochondrial activity. Here, we used MAS and PDH expression levels as surrogates of mitochondrial activity, because they are directly related to the two mitochondria-associated fluxes, J_N and J_{Ox}, in the model. Cell lines with less aerobic glycolysis (Fig. 3 *E*, *small blue circles*) distributed in the top right part where both growth rate and mitochondrial activity are high.

Reevaluation of the growth-rate-maximization hypothesis

After this analysis, the question of why proliferating cancer cells adopt flux configurations that favor aerobic glycolysis remains unclear. A commonly accepted hypothesis is that maximizing a biomass production flux (i.e., the growth rate) under some constraints on the fluxes leads to the Warburg effect. Our model challenges this hypothesis by revealing the possibility of proliferating fast without exhibiting the Warburg effect and an opposite relationship between growth rate and the Warburg effect. To further evaluate this hypothesis, we generated 2500 models under different combinations of upper limits for J_N ranging from 0.1 μmol/gWW/min to 5 μmol/gWW/min and J_{in} ranging from 0.2 μmol/gWW/min to 10 μmol/gWW/min, calculated the flux configuration maximizing the growth rate, μ, and the corresponding W (Fig. 4, *A* and *B*). Although maximizing μ under a majority of the models leads to nonzero lactate production, there exist models for which maximizing growth rate without aerobic glycolysis is possible. Adding randomly generated upper limits for the remaining fluxes and a random solvent-capacity constraint, i.e., the upper limit of the weighted sum of the fluxes (this implies that the flux configurations are limited by the capacity for the total amount of metabolic enzymes), resulted in even a larger fraction of the models maximizing growth rate without the necessity of the Warburg effect (Fig. 4 *C*). The results appear to imply that whether biomass production maximization leads to aerobic glycolysis depends on constraints (e.g., the maximal abundance of the enzymes or substrates) on the fluxes and needs more careful examination. In line with this, there is also evidence supporting the existence of rapidly proliferating cells without the Warburg effect (30,31).

DISCUSSION

To our knowledge, the equations for mass balance in glycolysis presented here show for the first time how the Warburg effect can be described analytically by a combination of a few fluxes using only a couple of parameters that have a clear biological interpretation. We were able to elucidate the origin of the Warburg effect and the interaction of fluxes in glycolysis and several related pathways using a relatively simple set of equations that are constrained by mass conservation in central carbon metabolism. Despite its extreme simplicity, the model is able to describe completely the Warburg effect and the fluxes needed to maintain the mechanisms that induce its form of metabolism.

From the derived relationships, it is apparent that the Warburg effect is determined by a combination of several fluxes,

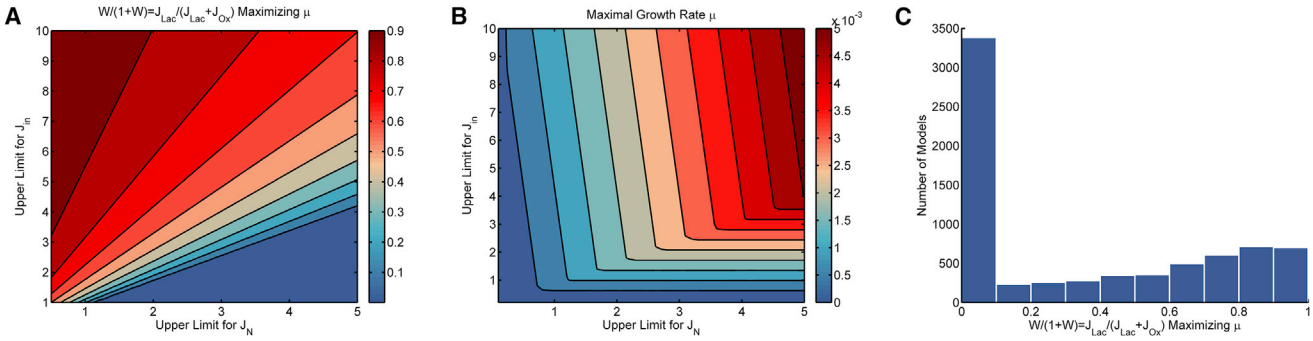

FIGURE 4 Maximization of biomass production may not lead to aerobic glycolysis. (*A*) Maximization of growth rate under different combinations of upper limits for J_N and J_{in} and the corresponding extent of the Warburg effect. $W/(1+W)$ was used instead of W for continuity. (*B*) Maximal growth rate under different combinations of upper limits for J_N and J_{in}. (*C*) Distribution of $W/(1+W)$ among 10000 randomly generated models maximizing growth rate under different combinations of the upper limits for all fluxes in the flux balance model with inclusion of a random solvent capacity constraint. To see this figure in color, go online.

including the rate of glucose uptake, ATP hydrolysis, and the extent of mitochondrial uncoupling of NADH turnover. The other variables involving redox regeneration, and the extent of biosynthesis, have constraints on their maximum rates. For example, the turnover of the redox status is limited by the rate of flux through the TCA cycle in the mitochondria.

Furthermore, our model demonstrates in exact terms the central role of redox balance in the Warburg effect by showing that although changing various fluxes in the model can lead to aerobic glycolysis, it is the demand to oxidize NADH produced in glycolysis and biomass synthesis, which cannot be oxidized by cytosolic NAD^+-regenerating enzymes alone, that entails aerobic glycolysis. The limited NAD^+-regenerating capacity not only leads to aerobic glycolysis under some conditions but also limits the cell's ability to increase flux passing biosynthesis pathways and supply growth. Consistently, inhibition of aspartate aminotransferase, which functions in the MAS, was reported to suppress growth in some cancer cells (32). Two recent studies reported that adding aspartate or other electron acceptors can restore proliferation in respiration-inhibited cells (33,34), which can be reflected in our model as relaxing the constraint on growth rate by increasing J_N.

Furthermore, when growth rate is coupled to two fluxes in the model, mechanisms for how growth rate is coupled to the Warburg effect are apparent. Nonzero lactate production is necessary under high growth rate when the cytosolic NAD^+-regenerating flux of the cell fails to oxidize all NADH generated in the glycolysis and biomass-synthesizing pathways. We expect that the conclusions on the role of redox balance in both regulating the Warburg effect and limiting the growth rate can be validated by experiments identifying the effect of perturbing J_N-related reactions, e.g., knockout of MAS-associated genes, or introduction of the redox-uncoupling agent α-ketobutyrate, on both growth rate and lactate production (33). For example, we showed in a recent work that knock down of MDH1 resulted in attenuation of the protective effect of exogenous lactate, thus supporting the role of J_N and J_{Lac} in keeping redox balance in the cytosol (35). Finally, we were able to construct the set of all feasible fluxes, which reflects the tight control of oxidative phosphorylation and the MAS over cellular growth rate.

The global flux-balance map also affords a clear illustration of how aerobic glycolysis is linked to growth rate and mitochondrial activity. According to the global-flux-balance map, growth rate, together with mitochondrial activity, affects the extent of the Warburg effect in a counterintuitive manner. Although some hypotheses on aerobic glycolysis consider it a consequence of adjusting cellular metabolism to satisfy energy and biomass requirements in proliferation (2,36), our analysis indicates a different trend. Due to the correlation between proliferation rate and mitochondrial activity, cells that proliferate faster often have more active mitochondria, thus exhibiting weaker aerobic glycolysis. We also showed that the Warburg effect may not be the result of maximization of biomass production by calculating flux configurations that maximize the growth rate under different combinations of upper limits of fluxes in the model.

Several assumptions, although apparent in certain settings, are not likely to be general. First, for some of the analysis, we assumed that growth rate is linear to flux of de novo serine synthesis, which is not always the case. Although various malignant cells rely on PHGDH for proliferation, the effect of PHGDH knockdown on proliferation varies among cell lines (37,38). Thus, J_{out} and μ are decoupled in many settings. Similarly, the assumption that ATP-hydrolyzing flux is linear to proliferation rate is not general. Nevertheless, replacing these linear equalities with a weaker association between the growth rates and serine-synthesizing or ATP-hydrolyzing fluxes is consistent with our conclusions on the proliferation-induced or redox-limited Warburg effect and the positive correlation among J_N, J_{Ox}, and μ (Fig S5). We also assumed that the fluxes are independent except for the constraints on balancing them, thus ignoring all signaling and genetic regulatory events that may introduce additional constraints by regulating multiple fluxes simultaneously. For example, the PI3K pathway regulates the activity of glycolytic enzymes, causing both upregulation of glycolysis and downregulation of flux entering mitochondria (4). Regarding the fluxes J_N and J_{Ox}, they are also correlated, since they are both associated with the mitochondria. However, each of these scenarios involving coregulation of coupled fluxes still obeys the mass balance constraints and results in points on the landscape. Since the main conclusions derived from the model are direct consequences of the equality and inequality constraints, they will remain unchanged even if we consider additional constraints. Energy sources other than glucose are also not considered in the model. We also demonstrated that further consideration of contributions from other energy sources like glutamine will not alter the conclusions by analyzing an alternative model allowing ATP to be produced from other sources (Fig S6). Another term that may affect the form of the model is the contribution of the NADH-transporting flux carried by the mitochondrial NADH shuttle to mitochondrial ATP production by oxidative phosphorylation, which appears as the third term in the J_A equation. Analysis of a modified model including this flux further supports the robustness of the main conclusions to variations in determining the accurate boundary of the model (Fig S7).

Correlating model predictions with transcriptomics data has limitations. Transcriptomics data are most abundant for both cell lines and human tissues, which are not amenable to further experimentation, but such data are limited by inherent difficulties in comparing them to metabolic fluxes due to low correlations between mRNA and protein levels (39) and other factors besides abundance of

enzymes in determining metabolic fluxes (e.g., posttranslational modification and allosteric regulation of enzymes).

To summarize, the flux-balance model of glycolysis presented here can be used to demonstrate the condition from which aerobic glycolysis arises. It revealed the central role of redox balance in inducing aerobic glycolysis, thus elucidating a plausible mechanism of redox-limited aerobic glycolysis. However, it doesn't exclude the possibility that cancer cells adopt the Warburg effect because the lactate production provides cell-inrinsic or cell-extrinsic benefits in some other way (5). The conclusions on the relationship between the Warburg effect and redox balance can be further validated by experiments showing how the Warburg effect and growth rate will respond to alterations in the redox state in cytosol.

SUPPORTING MATERIAL

Supporting Materials and Methods, seven figures, and two tables are available at http://www.biophysj.org/biophysj/supplemental/S0006-3495(16)30597-5

AUTHOR CONTRIBUTIONS

Z.D. and J.W.L. designed the study, conducted the research, and wrote the article with input from L.L. A.A.S. collected and analyzed the tissue data.

ACKNOWLEDGMENTS

J.W.L. thanks Danny Lew for insightful comments on the manuscript. Z.D. thanks Ning Yin for advice on the figures.

This work was supported in part by grants R01CA193256 and R00 CA168997 to J.W.L. from the National Cancer Institute at the National Institutes of Health, and grant 2015CB910300 to L.L. from the Ministry of Science and Technology of China.

SUPPORTING CITATIONS

References (40–77) appear in the Supporting Material.

REFERENCES

1. Racker, E. 1972. Bioenergetics and the problem of tumor growth. *Am. Sci.* 60:56–63.
2. Vander Heiden, M. G., L. C. Cantley, and C. B. Thompson. 2009. Understanding the Warburg effect: the metabolic requirements of cell proliferation. *Science.* 324:1029–1033.
3. Slavov, N., B. A. Budnik, …, A. van Oudenaarden. 2014. Constant growth rate can be supported by decreasing energy flux and increasing aerobic glycolysis. *Cell Reports.* 7:705–714.
4. Cairns, R. A., I. S. Harris, and T. W. Mak. 2011. Regulation of cancer cell metabolism. *Nat. Rev. Cancer.* 11:85–95.
5. Liberti, M. V., and J. W. Locasale. 2016. The Warburg effect: how does it benefit cancer cells? *Trends Biochem. Sci.* 41:211–218.
6. Vazquez, A., J. Liu, …, Z. N. Oltvai. 2010. Catabolic efficiency of aerobic glycolysis: the Warburg effect revisited. *BMC Syst. Biol.* 4:58.
7. Vazquez, A., and Z. N. Oltvai. 2011. Molecular crowding defines a common origin for the Warburg effect in proliferating cells and the lactate threshold in muscle physiology. *PLoS One.* 6:e19538.
8. Shlomi, T., T. Benyamini, …, E. Ruppin. 2011. Genome-scale metabolic modeling elucidates the role of proliferative adaptation in causing the Warburg effect. *PLOS Comput. Biol.* 7:e1002018.
9. Epstein, T., L. Xu, …, R. A. Gatenby. 2014. Separation of metabolic supply and demand: aerobic glycolysis as a normal physiological response to fluctuating energetic demands in the membrane. *Cancer Metab.* 2:7.
10. Pfeiffer, T., S. Schuster, and S. Bonhoeffer. 2001. Cooperation and competition in the evolution of ATP-producing pathways. *Science.* 292:504–507.
11. Shestov, A. A., B. Barker, …, J. W. Locasale. 2013. Computational approaches for understanding energy metabolism. *Wiley Interdiscip. Rev. Syst. Biol. Med.* 5:733–750.
12. Yizhak, K., B. Chaneton, …, E. Ruppin. 2015. Modeling cancer metabolism on a genome scale. *Mol. Syst. Biol.* 11:817.
13. Shestov, A. A., X. Liu, …, J. W. Locasale. 2014. Quantitative determinants of aerobic glycolysis identify flux through the enzyme GAPDH as a limiting step. *eLife.* 3:1–18.
14. Cline, M. S., B. Craft, …, J. Zhu. 2013. Exploring TCGA pan-cancer data at the UCSC Cancer Genomics Browser. *Sci. Rep.* 3:2652.
15. Goldman, M., B. Craft, …, J. Zhu. 2015. The UCSC Cancer Genomics Browser: update 2015. *Nucleic Acids Res.* 43:D812–D817.
16. Ogata, H., S. Goto, …, M. Kanehisa. 1999. KEGG: Kyoto encyclopedia of genes and genomes. *Nucleic Acids Res.* 27:29–34.
17. MOSEK ApS. 2015. The MOSEK Optimization Toolbox for MATLAB Manual, Version 7.1 (Revision 43). MOSEK ApS, Copenhagen, Denmark.
18. Madhukar, N. S., M. O. Warmoes, and J. W. Locasale. 2015. Organization of enzyme concentration across the metabolic network in cancer cells. *PLoS One.* 10:e0117131.
19. Putman, C. T., N. L. Jones, …, G. J. Heigenhauser. 1998. Effects of short-term submaximal training in humans on muscle metabolism in exercise. *Am. J. Physiol.* 275:E132–E139.
20. Taegtmeyer, H., R. Hems, and H. A. Krebs. 1980. Utilization of energy-providing substrates in the isolated working rat heart. *Biochem. J.* 186:701–711.
21. Bonen, A., K. J. McCullagh, …, G. J. Heigenhauser. 1998. Short-term training increases human muscle MCT1 and femoral venous lactate in relation to muscle lactate. *Am. J. Physiol.* 274:E102–E107.
22. Reinoso, R. F., B. A. Telfer, and M. Rowland. 1997. Tissue water content in rats measured by desiccation. *J. Pharmacol. Toxicol. Methods.* 38:87–92.
23. Kiricuta, I. C., Jr., and V. Simplăceanu. 1975. Tissue water content and nuclear magnetic resonance in normal and tumor tissues. *Cancer Res.* 35:1164–1167.
24. Locasale, J. W. 2013. Serine, glycine and one-carbon units: cancer metabolism in full circle. *Nat. Rev. Cancer.* 13:572–583.
25. Fan, J., J. Ye, …, J. D. Rabinowitz. 2014. Quantitative flux analysis reveals folate-dependent NADPH production. *Nature.* 510:298–302.
26. Labuschagne, C. F., N. J. F. van den Broek, …, O. D. K. Maddocks. 2014. Serine, but not glycine, supports one-carbon metabolism and proliferation of cancer cells. *Cell Reports.* 7:1248–1258.
27. Kilburn, D. G., M. D. Lilly, and F. C. Webb. 1969. The energetics of mammalian cell growth. *J. Cell Sci.* 4:645–654.
28. Locasale, J. W., and L. C. Cantley. 2011. Metabolic flux and the regulation of mammalian cell growth. *Cell Metab.* 14:443–451.
29. Jain, M., R. Nilsson, …, V. K. Mootha. 2012. Metabolite profiling identifies a key role for glycine in rapid cancer cell proliferation. *Science.* 336:1040–1044.
30. Lee, M., and J.-H. Yoon. 2015. Metabolic interplay between glycolysis and mitochondrial oxidation: the reverse Warburg effect and its therapeutic implication. *World J. Biol. Chem.* 6:148–161.
31. Hensley, C. T., B. Faubert, …, R. J. DeBerardinis. 2016. Metabolic heterogeneity in human lung tumors. *Cell.* 164:681–694.

32. Thornburg, J. M., K. K. Nelson, …, J. Chesney. 2008. Targeting aspartate aminotransferase in breast cancer. *Breast Cancer Res.* 10:R84.

33. Sullivan, L. B., D. Y. Gui, …, M. G. Vander Heiden. 2015. Supporting aspartate biosynthesis is an essential function of respiration in proliferating cells. *Cell.* 162:552–563.

34. Birsoy, K., T. Wang, …, D. M. Sabatini. 2015. An essential role of the mitochondrial electron transport chain in cell proliferation Is to enable aspartate synthesis. *Cell.* 162:540–551.

35. Park, S., C.-Y. Chang, …, D. P. McDonnell. 2016. ERRα-regulated lactate metabolism contributes to resistance to targeted therapies in breast cancer. *Cell Reports.* 15:323–335.

36. Basan, M., S. Hui, …, T. Hwa. 2015. Overflow metabolism in *Escherichia coli* results from efficient proteome allocation. *Nature.* 528: 99–104.

37. Locasale, J. W., A. R. Grassian, …, M. G. Vander Heiden. 2011. Phosphoglycerate dehydrogenase diverts glycolytic flux and contributes to oncogenesis. *Nat. Genet.* 43:869–874.

38. Possemato, R., K. M. Marks, …, D. M. Sabatini. 2011. Functional genomics reveal that the serine synthesis pathway is essential in breast cancer. *Nature.* 476:346–350.

39. Maier, T., M. Güell, and L. Serrano. 2009. Correlation of mRNA and protein in complex biological samples. *FEBS Lett.* 583:3966–3973.

40. Hinkle, P. C. 2005. P/O ratios of mitochondrial oxidative phosphorylation. *Biochim. Biophys. Acta.* 1706:1–11.

41. Du, F., X. H. Zhu, …, W. Chen. 2007. Efficient in vivo ^{31}P magnetization transfer approach for noninvasively determining multiple kinetic parameters and metabolic fluxes of ATP metabolism in the human brain. *Magn. Reson. Med.* 57:103–114.

42. Lei, H., K. Ugurbil, and W. Chen. 2003. Measurement of unidirectional Pi to ATP flux in human visual cortex at 7 T by using in vivo ^{31}P magnetic resonance spectroscopy. *Proc. Natl. Acad. Sci. USA.* 100:14409–14414.

43. Shoubridge, E. A., R. W. Briggs, and G. K. Radda. 1982. ^{31}p NMR saturation transfer measurements of the steady state rates of creatine kinase and ATP synthetase in the rat brain. *FEBS Lett.* 140:289–292.

44. Du, F., X.-H. Zhu, …, W. Chen. 2008. Tightly coupled brain activity and cerebral ATP metabolic rate. *Proc. Natl. Acad. Sci. USA.* 105:6409–6414.

45. Petersen, K. F., D. Befroy, …, G. I. Shulman. 2003. Mitochondrial dysfunction in the elderly: possible role in insulin resistance. *Science.* 300:1140–1142.

46. Befroy, D. E., K. F. Petersen, …, G. I. Shulman. 2008. Increased substrate oxidation and mitochondrial uncoupling in skeletal muscle of endurance-trained individuals. *Proc. Natl. Acad. Sci. USA.* 105: 16701–16706.

47. Brindle, K. M., M. J. Blackledge, …, G. K. Radda. 1989. ^{31}P NMR magnetization-transfer measurements of ATP turnover during steady-state isometric muscle contraction in the rat hind limb in vivo. *Biochemistry.* 28:4887–4893.

48. van den Broek, N. M. A., J. Ciapaite, …, J. J. Prompers. 2010. Comparison of in vivo postexercise phosphocreatine recovery and resting ATP synthesis flux for the assessment of skeletal muscle mitochondrial function. *Am. J. Physiol. Cell Physiol.* 299:C1136–C1143.

49. Jucker, B. M., S. Dufour, …, G. I. Shulman. 2000. Assessment of mitochondrial energy coupling in vivo by ^{13}C/^{31}P NMR. *Proc. Natl. Acad. Sci. USA.* 97:6880–6884.

50. Cline, G. W., A. J. Vidal-Puig, …, G. I. Shulman. 2001. In vivo effects of uncoupling protein-3 gene disruption on mitochondrial energy metabolism. *J. Biol. Chem.* 276:20240–20244.

51. Schmid, A. I., M. Chmelík, …, M. Roden. 2008. Quantitative ATP synthesis in human liver measured by localized ^{31}P spectroscopy using the magnetization transfer experiment. *NMR Biomed.* 21:437–443.

52. Thoma, W. J., and K. Uğurbil. 1987. Saturation-transfer studies of ATP-Pi exchange in isolated perfused rat liver. *Biochim. Biophys. Acta.* 893:225–231.

53. Matthews, P. M., J. L. Bland, …, G. K. Radda. 1981. The steady-state rate of ATP synthesis in the perfused rat heart measured by ^{31}P NMR saturation transfer. *Biochem. Biophys. Res. Commun.* 103:1052–1059.

54. Kingsley-Hickman, P. B., E. Y. Sako, …, K. Uğurbil. 1987. ^{31}P NMR studies of ATP synthesis and hydrolysis kinetics in the intact myocardium. *Biochemistry.* 26:7501–7510.

55. Gruetter, R., E. R. Seaquist, and K. Ugurbil. 2001. A mathematical model of compartmentalized neurotransmitter metabolism in the human brain. *Am. J. Physiol. Endocrinol. Metab.* 281:E100–E112.

56. Duarte, J. M. N., and R. Gruetter. 2013. Glutamatergic and GABAergic energy metabolism measured in the rat brain by ^{13}C NMR spectroscopy at 14.1 T. *J. Neurochem.* 126:579–590.

57. Boumezbeur, F., L. Besret, …, V. Lebon. 2005. Glycolysis versus TCA cycle in the primate brain as measured by combining ^{18}F-FDG PET and ^{13}C-NMR. *J. Cereb. Blood Flow Metab.* 25:1418–1423.

58. Boumezbeur, F., L. Besret, …, V. Lebon. 2004. NMR measurement of brain oxidative metabolism in monkeys using ^{13}C-labeled glucose without a ^{13}C radiofrequency channel. *Magn. Reson. Med.* 52:33–40.

59. Ziegler, A., C. E. Zaugg, …, B. Künnecke. 2002. Non-invasive measurements of myocardial carbon metabolism using in vivo ^{13}C NMR spectroscopy. *NMR Biomed.* 15:222–234.

60. Chance, E. M., S. H. Seeholzer, …, J. R. Williamson. 1983. Mathematical analysis of isotope labeling in the citric acid cycle with applications to ^{13}C NMR studies in perfused rat hearts. *J. Biol. Chem.* 258:13785–13794.

61. Chatham, J. C., J. R. Forder, …, E. M. Chance. 1995. Calculation of absolute metabolic flux and the elucidation of the pathways of glutamate labeling in perfused rat heart by ^{13}C NMR spectroscopy and nonlinear least squares analysis. *J. Biol. Chem.* 270:7999–8008.

62. O'Donnell, J. M., K. Pound, …, E. D. Lewandowski. 2009. SERCA1 expression enhances the metabolic efficiency of improved contractility in post-ischemic heart. *J. Mol. Cell. Cardiol.* 47:614–621.

63. Sorokina, N., J. M. O'Donnell, …, E. D. Lewandowski. 2007. Recruitment of compensatory pathways to sustain oxidative flux with reduced carnitine palmitoyltransferase I activity characterizes inefficiency in energy metabolism in hypertrophied hearts. *Circulation.* 115:2033–2041.

64. Yu, X., L. T. White, …, E. D. Lewandowski. 1996. Subcellular metabolite transport and carbon isotope kinetics in the intramyocardial glutamate pool. *Biochemistry.* 35:6963–6968.

65. Jeffrey, F. M., C. J. Storey, …, C. R. Malloy. 1996. ^{13}C isotopomer model for estimation of anaplerotic substrate oxidation via acetyl-CoA. *Am. J. Physiol.* 271:E788–E799.

66. Befroy, D. E., K. F. Petersen, …, G. I. Shulman. 2007. Impaired mitochondrial substrate oxidation in muscle of insulin-resistant offspring of type 2 diabetic patients. *Diabetes.* 56:1376–1381.

67. Myles, D. D., P. Strong, and M. C. Sugden. 1984. Errors arising from the use of [$^{1-14}$C]pyruvate to measure flux through the liver pyruvate dehydrogenase complex. *Biochem. J.* 218:997–998.

68. Gruetter, R., E. J. Novotny, …, R. G. Shulman. 1996. ^{1}H NMR studies of glucose transport in the human brain. *J. Cereb. Blood Flow Metab.* 16:427–438.

69. Shestov, A. A., U. E. Emir, …, G. Öz. 2011. Simultaneous measurement of glucose transport and utilization in the human brain. *Am. J. Physiol. Endocrinol. Metab.* 301:E1040–E1049.

70. Pan, J. W., D. T. Stein, …, H. P. Hetherington. 2000. Spectroscopic imaging of glutamate C4 turnover in human brain. *Magn. Reson. Med.* 44:673–679.

71. Duarte, J. M. N., and R. Gruetter. 2012. Characterization of cerebral glucose dynamics in vivo with a four-state conformational model of transport at the blood-brain barrier. *J. Neurochem.* 121:396–406.

72. Dimitriadis, G., P. Mitrou, …, S. A. Raptis. 2008. Insulin-stimulated rates of glucose uptake in muscle in hyperthyroidism: the importance of blood flow. *J. Clin. Endocrinol. Metab.* 93:2413–2415.

73. Knuuti, M. J., P. Nuutila, …, L.-M. Voipio-Pulkki. 1993. The value of quantitative analysis of glucose utilization in detection of myocardial viability by PET. *J. Nucl. Med.* 34:2068–2075.

74. Forbes, N. S., A. L. Meadows, …, H. W. Blanch. 2006. Estradiol stimulates the biosynthetic pathways of breast cancer cells: detection by metabolic flux analysis. *Metab. Eng.* 8:639–652.

75. Cakir, T., S. Alsan, …, K. O. Ulgen. 2007. Reconstruction and flux analysis of coupling between metabolic pathways of astrocytes and neurons: application to cerebral hypoxia. *Theor. Biol. Med. Model.* 4:48.

76. Lu, M., L. Zhou, …, X. Yu. 2008. Role of the malate-aspartate shuttle on the metabolic response to myocardial ischemia. *J. Theor. Biol.* 254:466–475.

77. Lu, M., S. Banerjee, …, X. Yu. 2011. Regulation of cytosolic and mitochondrial oxidation via malate-aspartate shuttle: an observation using dynamic ^{13}C NMR spectroscopy. *Adv. Exp. Med. Biol.* 701:185–192.